Pictorial Essay

J Korean Soc Radiol 2024;85(2):345-362
https://doi.org/10.3348/jksr.2023.0067
eISSN 2951-0805

JOURNAL of THE KOREAN SOCIETY of RADIOLOGY

Advanced Abdominal MRI Techniques and Problem-Solving Strategies

복부 자기공명영상 고급 기법과 문제 해결 전략

Yoonhee Lee, MD[1], Sungjin Yoon, MD[1],
So Hyun Park, MD[1*], Marcel Dominik Nickel, PhD[2]

[1]Department of Radiology, Gil Medical Center, Gachon University College of Medicine, Incheon, Korea
[2]MR Application Predevelopment, Siemens Healthcare GmbH, Erlangen, Germany

Received June 5, 2023
Revised October 4, 2023
Accepted October 14, 2023

***Corresponding author**
So Hyun Park, MD
Department of Radiology,
Gil Medical Center,
Gachon University
College of Medicine,
21 Namdong-daero 774beon-gil,
Namdong-gu, Incheon 21565,
Korea.

Tel 82-32-460-3060
Fax 82-32-460-3065
E-mail nnoleeter@gilhospital.com

MRI plays an important role in abdominal imaging because of its ability to detect and characterize focal lesions. However, MRI examinations have several challenges, such as comparatively long scan times and motion management through breath-holding maneuvers. Techniques for reducing scan time with acceptable image quality, such as parallel imaging, compressed sensing, and cutting-edge deep learning techniques, have been developed to enable problem-solving strategies. Additionally, free-breathing techniques for dynamic contrast-enhanced imaging, such as extra-dimensional-volumetric interpolated breath-hold examination, golden-angle radial sparse parallel, and liver acceleration volume acquisition Star, can help patients with severe dyspnea or those under sedation to undergo abdominal MRI. We aimed to present various advanced abdominal MRI techniques for reducing the scan time while maintaining image quality and free-breathing techniques for dynamic imaging and illustrate cases using the techniques mentioned above. A review of these advanced techniques can assist in the appropriate interpretation of sequences.

Index terms Magnetic Resonance Imaging; MRI Scan; Deep Learning Reconstruction; Liver

INTRODUCTION

Over the last 30 years, several advances have been made in the field of MRI in various respects. Great progress in data acquisition, image reconstruction, and postprocessing has contributed to the widespread use of MRI in the clinical setting (1). However, MRI examinations require at least 20–30 minutes, or in certain cases even 60 minutes or longer, for complex studies. Long examination times result in poor image quality owing to inevitable motion artifacts. Abdominal MRI findings can be easily affected by a patient's breathing status. Moreover, liver-specific contrast agents (e.g., gadoxetic acid) in con-

JOURNAL of THE KOREAN SOCIETY of RADIOLOGY

trast-enhanced liver MRI may cause transient severe motion artifacts after injection, and capturing an optimal arterial phase scan timing is not easy (2, 3). Parallel imaging, compressed sensing (CS), and deep learning (DL) techniques were introduced to enable problem-solving strategies. For example, applying parallel imaging in MRI enables a reduction in the scan time by achieving linear undersampling of the phase-encoding direction in k-space. However, using a high acceleration factor can result in remnant aliasing artifacts and poor signal-to-noise ratio (SNR). Another fast imaging technique is CS, which requires sparsity, incoherent undersampling, and non-linear iterative reconstruction to accelerate the MRI acquisition. Optimizing the regularization and acceleration factors can be challenging when applying a CS. To solve these problems, DL techniques have recently been introduced for image reconstruction. Therefore, we reviewed various advanced MRI techniques (Table 1) to reduce scan time, while maintaining comparable image quality and enabling free-breathing examinations.

PARALLEL IMAGING

The MRI scan time is directly related to k-space sampling, a technique that reconstructs images from partially sampled k-space data reducing the scan time. Parallel imaging is also commonly performed. This approach relied on the acquisition of multiple receiver coils (4). The data acquired simultaneously via phased-array coils and the corresponding sensitivity profiles can be utilized in image reconstruction. In conventional parallel imaging, k-space is undersampled by skipping phase-encoding lines and acquiring them with larger equidistant steps (Fig. 1) (5). Although the image acquisition time is shortened proportionally to the acceleration factor, which specifies the reduction in acquired phase-encoding steps, the acquisition

Table 1. Techniques for Rapid Abdominal MRI

Technique	Clinical Application	Advantages	Drawbacks	K-Space Sampling
Parallel imaging	Applied in most pulse sequences (T2WI, DWI) and combined with other time–reduction strategies (T1WI)	Reducing scan time proportional to the AF Removing aliasing artifacts	Poor SNR or residual aliasing artifact with a high AF (> 4)	Cartesian sampling; phase-encoding direction
3D acceleration acquisition	T1WI	Using a higher AF than parallel imaging while maintaining image quality	Poor SNR with a high AF (> 5)	Cartesian sampling; phase, partition-encoding direction
Compressed sensing	Reducing image scan time, usually well applied in 3D MRCP, T1WI, and MRE	Reducing scan time with a higher AF (AF > 4) or thin-section scanning Better SNR than parallel imaging	Increased non-respiratory artifacts Synthetic appearance when excessive regularization factor	Pseudo-random subsampling
Deep learning	Applied for T2WI, DWI, contrast enhanced T1WI	Markedly reducing scan time with maintaining optimal image quality	Validation state	Highly undersampled Catesian sampling

AF = acceleration factor, DWI = diffusion weighted imaging, MRE = MR enterography, MRCP = MR cholangiopancreatography, SNR = signal-noise-ratio, T1WI = T1 weighted imaging, T2WI = T2 weighted imaging

corresponds to a reduced field of view (FOV). Furthermore, spatial aliasing artifacts due to imperfect modeling of receiver coil characteristics can occur at a high acceleration factor (4).

Parallel-imaging techniques are generally classified into two groups. The main difference is whether image reconstruction and artifact correction are performed for the aliased image (image domain after Fourier transformation) or the undersampled k-space data (k-space domain before Fourier transformation). For example, sensitivity encoding (SENSE) and array spatial sensitivity encoding techniques (ASSET), developed respectively by Philips Healthcare in the Best, Netherlands and GE Healthcare in Waukesha, Wisconsin, WI, USA, operate with aliased images. On the other hand, generalized auto-calibrating partially parallel acquisition (GRAPPA) and auto-calibrating reconstruction for Cartesian imaging (ARC), developed by Siemens Healthineers in Erlangen, Germany, and GE Healthcare, reconstruct an image by calculating unacquired k-space data (Fig. 2A, B) (4, 5).

The first approach (SENSE, ASSET) works on aliased images from each coil after calculating the coil sensitivities. For a k-space-based parallel imaging technique (GRAPPA, ARC), the correlation between coil elements is used to interpolate the missing k-space data before Fourier transformation (5, 6).

Parallel imaging techniques decrease the echo-train length in single-shot fast spin-echo (SSFSE) images, thereby decreasing both the readout and effective echo time (TE). This reduction effectively mitigates the blurring artifacts caused by T2 and T2* effects (Fig. 2C, D) (7, 8). A main drawback of parallel imaging is caused by undersampling parallel lines in two-dimensional imaging at a high ($\geq$ 4) acceleration. This leads to poor SNR escalated noise level, and residual aliasing artifacts (9). In the three-dimensional (3D) acceleration acquisition technique, two dimensions are undersampled, which improves the SNR while using a high acceleration factor (e.g., 4, or 5). The CS technique applies a high acceleration factor (> 4, e.g., 8 or 20) through pseudorandom undersampling for advanced rapid imaging (5).

3D ACCELERATION ACQUISITION TECHNIQUE

In the 3D acceleration acquisition technique, the two dimensions were undersampled in parallel lines (5). Parallel imaging techniques involve linear k-space undersampling in the

Fig. 1. Representative diagrams of k-space sampling.
A-C. Fully sampled k-space (A), parallel imaging (B), and compressed sensing (C).

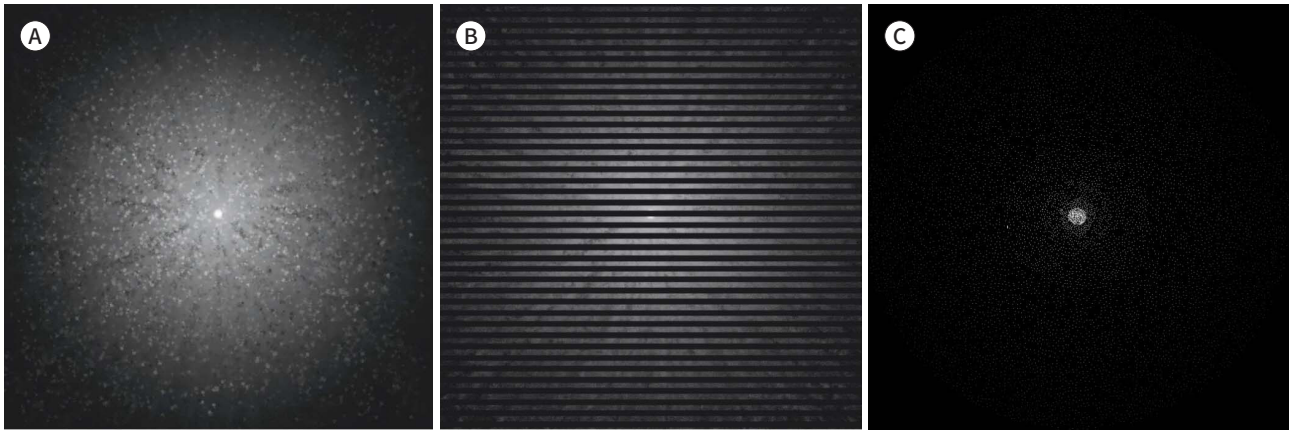

JOURNAL of THE KOREAN SOCIETY of RADIOLOGY

Fig. 2. T2-weighted images using parallel imaging (A-C) and not using parallel imaging (D).
A, B. First image (A) and fat-suppressed images (B) were obtained with T2 HASTE with partial Fourier factor 5/8 and image acquisition time if both are 1 minute (acceleration factor, 2, respectively), and both display comparable image quality and spatial resolution (reconstructed voxel size A: 0.5 × 0.5 × 5.0 mm^3, B: 0.6 × 0.6 × 5.0 mm^3).
C, D. HASTE with parallel imaging (C) (GRAPPA, acceleration factor phase encoding 2, voxel size 0.5 × 0.5 × 5.0 mm^3, TR 1000 ms, TE 88 ms, matrix 384 × 312, FOV 360 × 293, partial Fourier factor 5/8) and without parallel imaging (D) (TR 1200 ms, TE 88 ms, matrix 384 × 312, FOV 360 × 293, partial Fourier factor 4/8). Without parallel imaging, the image displays increasing blurring artifacts due to longer echo-train lengths (D).
*All figures were obtained using a 3T scanner (MAGNETOM Vida; Siemens Healthcare, Erlangen, Germany).
FOV = field of view, GRAPPA = generalized auto-calibrating partially parallel acquisition, HASTE = half Fourier single-shot turbo spin-echo, TE = echo time, TR = repetition time

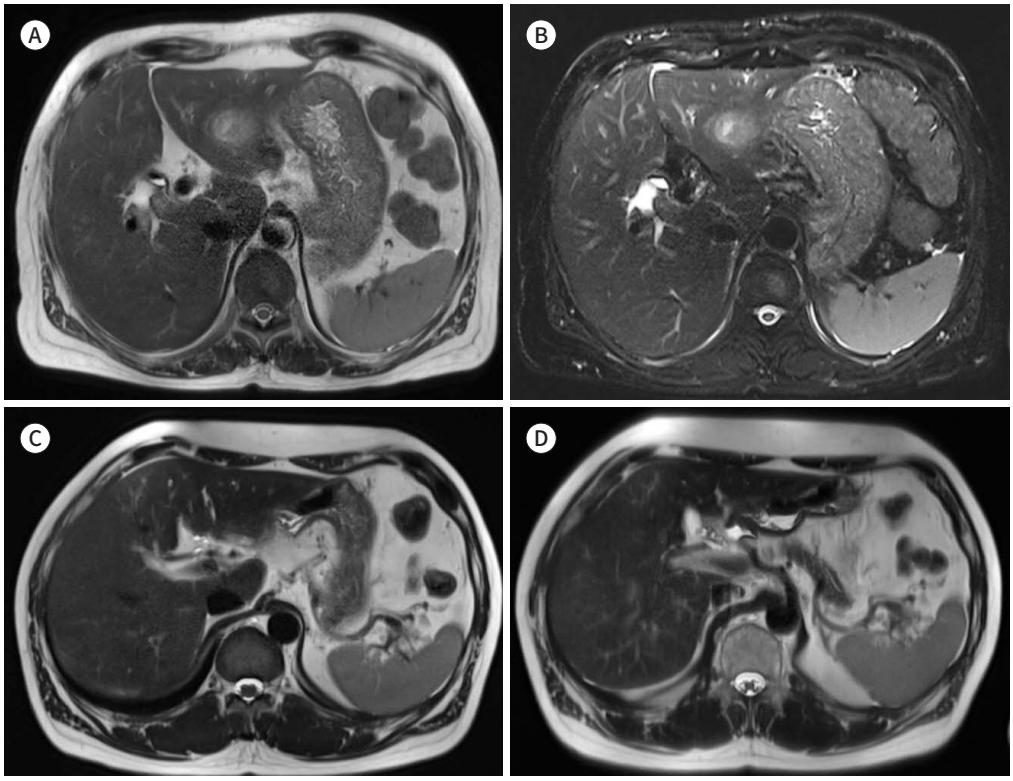

phase-encoding direction, whereas 3D acceleration acquisition techniques involve undersampling in both partition and phase-encoding directions. Undersampling in both directions can effectively reduce noise amplification and aliasing artifacts (4). However, if the slice direction is regularly undersampled, the probability of aliasing artifacts increases. The reordering shift technique, a method known as generalized-to-controlled aliasing in parallel imaging (CAIPIRINHA, Siemens Healthineers), can minimize aliasing artifacts. CAIPIRINHA improves the image quality of the hepatic arterial phase in gadoxetic acid-enhanced liver MRI (10). Specifically, the partitions acquired at a given line are shifted relative to those at the previously acquired line by the reordering shift delta (δ) (11). Therefore, δ is smaller than the acceleration factor in the partition direction. Changing the sampling pattern regularly shifts aliasing artifacts and allows better exploitation of the coil geometry for a given setup (10). This method enables a high acceleration factor and reduces the image acquisition time while maintaining imaging quality (Fig. 3).

COMPRESSED SENSING

Moreover, CS is another technique for reducing image acquisition time by 'compressing' the MRI acquisition. Although every image is compressible, determining the parts that are essential or redundant in medical images is important. To reconstruct a compressed image from as little data as possible, certain prerequisites are necessary: sparsity in a transform domain to be compressible, incoherent (random) k-space sampling resulting in noise-like aliasing artifacts, and non-linear iterative reconstruction for enforcing sparsity as well as data consistency (12). A CS with a high acceleration factor exhibits a reduced scan time with comparable image quality or thin-section scanning with a similar acquisition time (Fig. 4) (13).

Random (in fact, pseudo-random) sampled k-space intuitively adds incoherent aliasing artifacts to the image (12). A sparsity transformation, such as wavelets, translates the image into a transform domain, where the regularization factor determines the denoising. After several iterations to check data consistency, the final reconstructed image was acquired (14, 15). When the regularization factor increased, the SNR of the reconstructed images improved. However, at the same time, the artificial appearance of an image would be emphasized and fine structures might be over-smoothed (16). These regularization factors in CS cannot be automated

Fig. 3. Dual arterial phase images in a 67-year-old female.
Images were obtained using CAIPIRINHA with an acceleration factor of 5 (acceleration factor phase encoding 1, acceleration factor 3D 5, Reordering shift 3D 2) and 0.5 × 0.5 × 3.0 mm^3 voxel size.
A. The first image was obtained in the early arterial phase.
B. The next image was obtained in the late arterial phase. Image acquisition time is 14 seconds in total including a preparation scan of 2 seconds, and two arterial phases (each 6 seconds, respectively).
C, D. Subtraction arterial phase images were reconstructed using (A, B) images and pre-contrast images in early and late arterial phases.
CAIPIRINHA = controlled aliasing in parallel imaging results in higher acceleration

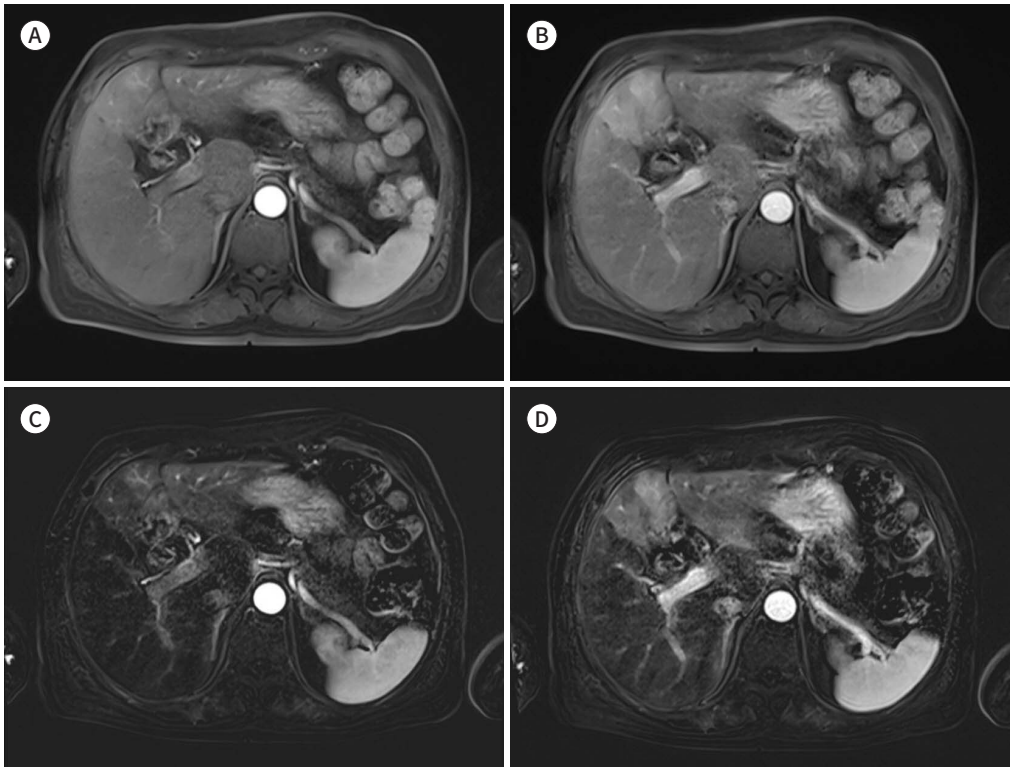

JOURNAL of THE KOREAN SOCIETY of RADIOLOGY

(17). Although incoherent and aliasing artifacts are theoretically removed during iterative reconstruction, a few studies have identified that ringing artifacts and blurring of fine details may be visible in CS (Fig. 5) (18).

Fig. 4. Hepatobiliary phase using CAIPIRINHA and compressed sensing in gadoxetic acid-enhanced liver MRI in a 63-year-old male with liver cirrhosis and chronic hepatitis B.
A. First hepatobiliary phase image was obtained using CAIPIRINHA with an acceleration factor of 4 (acceleration factor phase encoding 2, acceleration factor 3D 2, reordering shift 3D 1; reconstructed voxel size, $1.3 \times 1.3 \times 3.0$ mm^3, image acquisition time, 16 seconds).
B. Next hepatobiliary phase image was obtained using compressed sensing with acceleration factor of 8 (reconstructed voxel size, $0.9 \times 0.9 \times 1.5$ mm^3, image acquisition time, 15 seconds). Non-respiratory motion artifacts are visible in the image (arrows), which slightly decreases overall image quality.
CAIPIRINHA = controlled aliasing in parallel imaging results in higher acceleration

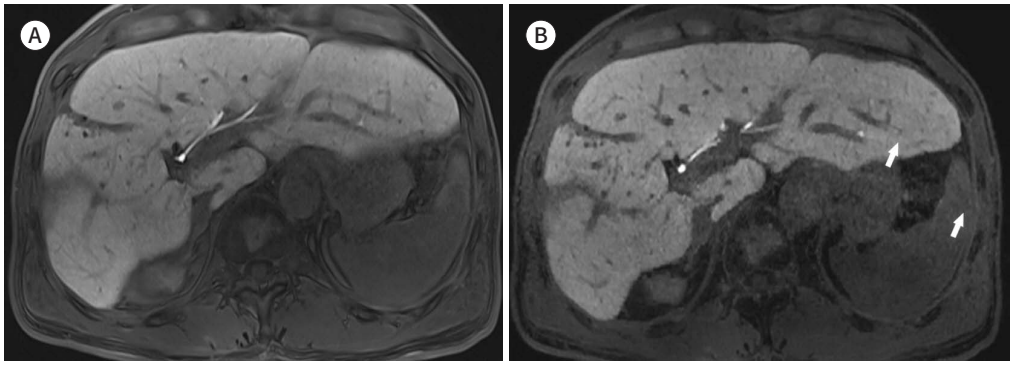

Fig. 5. Non-respiratory motion artifacts using a compressed sensing research application on hepatobiliary phase (reconstructed voxel size, $0.9 \times 0.9 \times 1.5$ mm^3; total acceleration factor of 8) of gadoxetic acid-enhanced liver MRI.
A, B. Hepatobiliary phase images in a 61-year-old male with chronic hepatitis C display moderate non-respiratory artifacts related to incoherent sampling (arrows).
C. The hepatobiliary phase image in a 61-year-old male with liver cirrhosis displays non-respiratory artifacts including cardiac ghosting artifact (arrow) in the left lateral segment.
D, E. The hepatobiliary phase in a 62-year-old male with liver cirrhosis and chronic hepatitis B displays non-respiratory artifacts including ringing artifacts (arrow, magnification image).

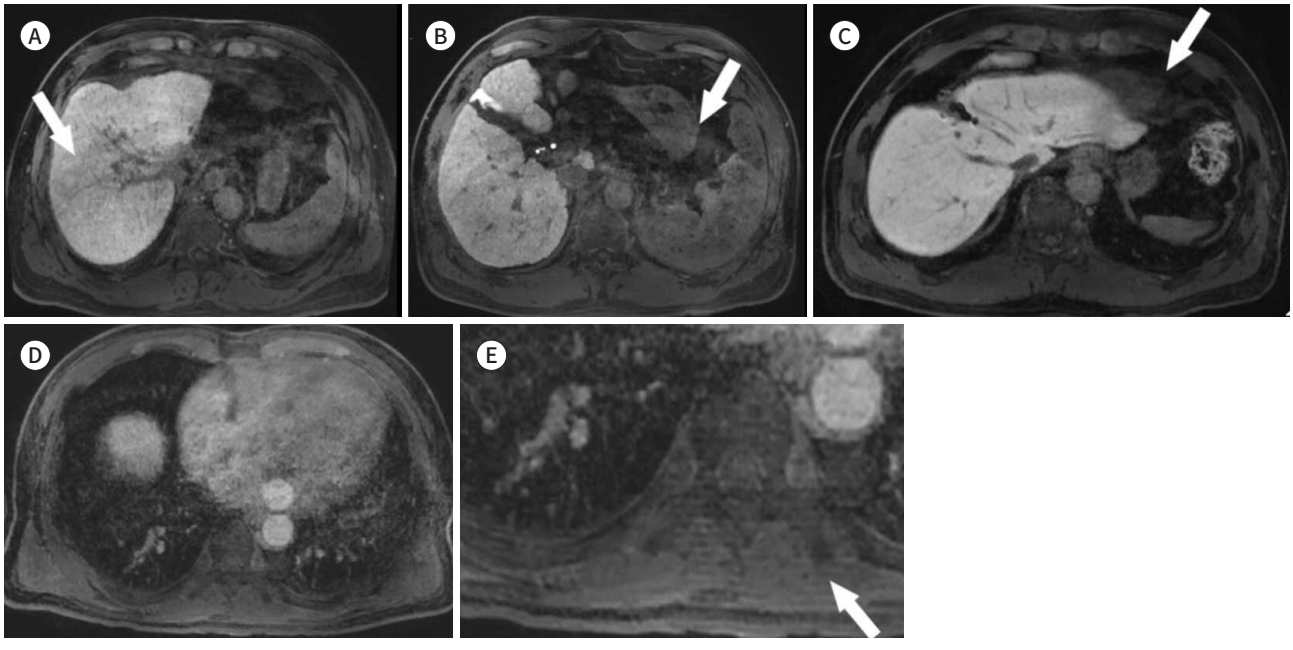

In cases of high sparsity in the image domain, such as in 3D MR cholangiopancreatography (MRCP) CS is effectively applied (Fig. 6). Moreover, 3D MRCP displays a high contrast of fluid-containing structures, such as the bile and pancreatic duct, while suppressing any other background signals. This sparsity in the image domain enables the maximization of the use of a CS technique with reduced scan time (5). Although conventional respiratory-triggered MRCP requires a significant scan duration of approximately 7 min, breath-hold compressed-sensing 3D MRCP substantially reduces the scan time to less than 20 s (with acceleration factors ranging from 17 to 28) (19-21). Additionally, the diagnostic modality offers moderate to high accuracy for evaluating the bile and pancreatic ducts (21).

DEEP LEARNING

As discussed above, several acceleration techniques, such as parallel imaging and CS, have been introduced in clinical practice. Additionally, CS demonstrates better SNR than parallel imaging but may oversimplify the image content, resulting in residual blurring and loss of texture (22). In recent years, DL-based imaging has been studied for the further acceleration of MRI. This technique has the potential to markedly reduce the scan time while maintaining optimal image quality (23).

DL can be applied along lines to reduce acquisition time and improve image quality while maintaining data consistency (24, 25). Two main methods are available: image-to-image deep neural networks and k-space-to-image deep neural networks (Figs. 7-9). In image-based DL, image denoising and super-resolution can be used for image enhancement. Image denoising can be used for images with aliasing artifacts or other nonspecific noise in a zero-filled reconstructed image acquired from the undersampled k-space (24). Noise maps calculated from the adjustment information can be used to guide adaptive denoising. Super-resolution

Fig. 6. MR cholangiopancreatography images in a 67-year-old female with chronic pancreatitis.
A. The first image was obtained using CAIPIRINHA with an acceleration factor of 4 (acceleration factor phase encoding 2, acceleration factor 3D 2, reordering shift 3D 1).
B. The next image was obtained using compressed sensing with an acceleration factor of 25. Although both images display comparable image quality and spatial resolution (reconstructed voxel size A: 0.5 × 0.5 × 1.0 mm^3, B: 0.5 × 0.5 × 0.9 mm^3), image acquisition time is 3 minutes 46 seconds in (A) and 18 seconds in (B).

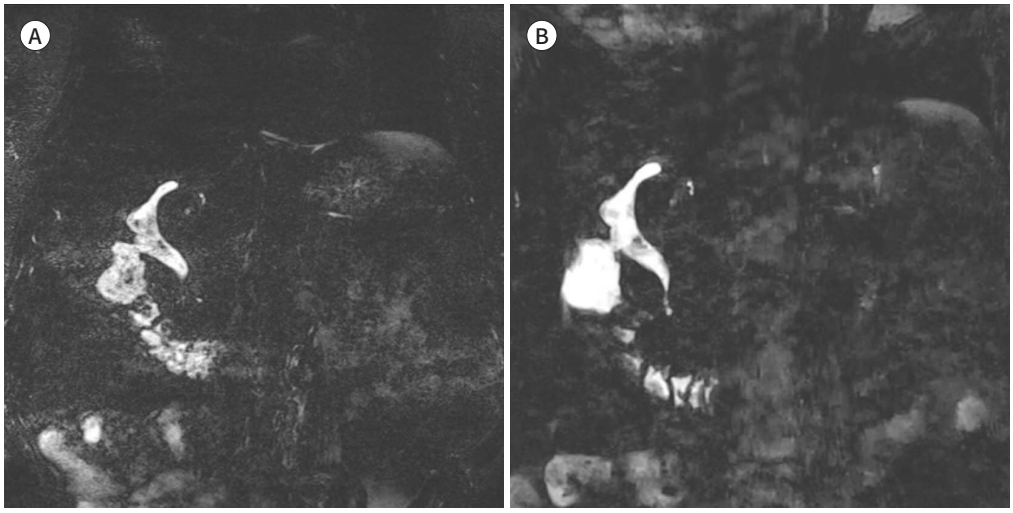

JOURNAL of THE KOREAN SOCIETY of RADIOLOGY

aims to improve low-resolution images towards a high resolution in terms of sharpness and contrast enabled by image-based DL (26). Furthermore, DL-based reconstructions from neural networks trained on representative data provide optimal image quality (Deep Resolved

Fig. 7. Hepatobiliary phase using CAIPIRINHA and DL in gadoxetic acid-enhanced liver MRI in a 57-year-old man with chronic hepatitis B.
A-C. Images were obtained using CAIPIRINHA with an acceleration factor of 4 (acceleration factor phase encoding 2, acceleration factor 3D 2, reordering shift 3D 1; 16 seconds; matrix 384 × 270).
D-F. Images were obtained with a research DL reconstruction (k-space DL reconstruction) and CAIPIRINHA with an acceleration factor of 6 (acceleration factor phase encoding 3, acceleration factor 3D 2, reordering shift 3D 1; 12 seconds; matrix 448 × 276).
CAIPIRINHA = controlled aliasing in parallel imaging results in higher acceleration, DL = deep-learning

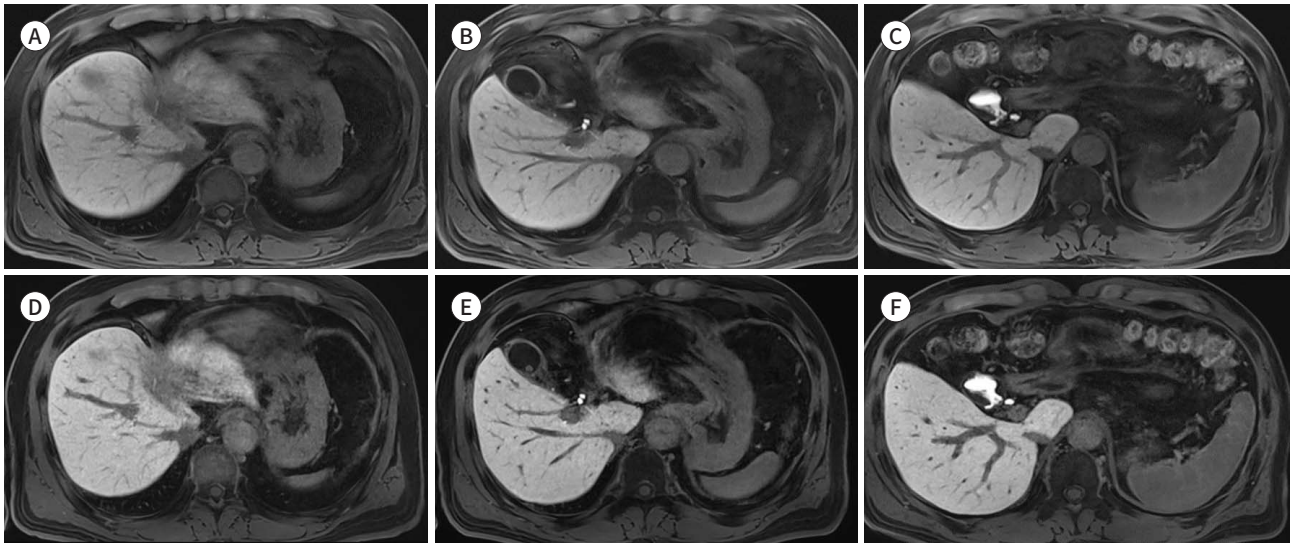

Fig. 8. T2-weighted images using T2 HASTE and DL in liver MRI in a 45-year-old male with liver cirrhosis and chronic hepatitis C.
A-C. Images were obtained with HASTE (GRAPPA; acceleration factor 2; acquisition time 60 seconds; matrix 320 × 221; partial Fourier factor 7/8; reconstructed voxel size, 1.3 × 1.3 × 5.0 mm^3).
D-F. DL images were obtained using HASTE (acceleration factor 3; acquisition time 55 seconds; 384 × 218; partial Fourier factor 7/8; 0.5 × 0.5 × 5.0 mm^3) with a research DL reconstruction. Although DL HASTE displays high spatial resolution with improved edge sharpness and reduced noise, it was obtained with a short image acquisition time compared to HASTE without DL.
DL = deep-learning, HASTE = half-Fourier acquisition single-shot turbo spin-echo

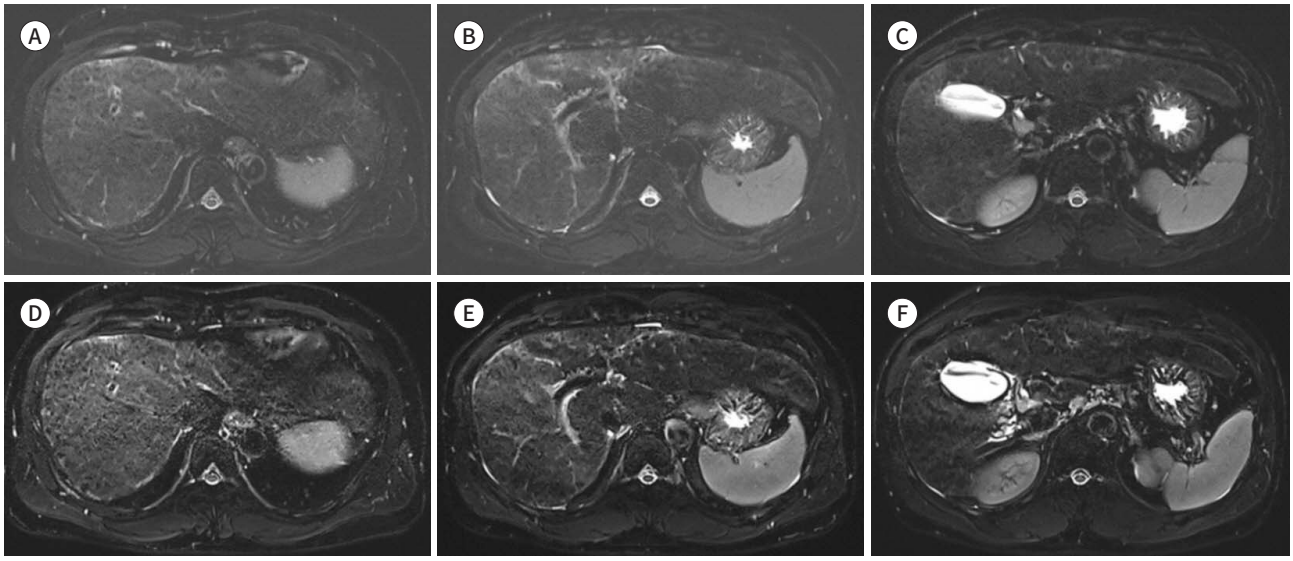

Fig. 9. T2-weighted images using BLADE with DL reconstruction in liver MRI in a 71-year-old male with hepatic metastasis.
A. The image was obtained with BLADE (GRAPPA; acceleration factor 3; 16 minutes; matrix 320 × 320; partial Fourier factor 7/8; reconstructed voxel size, 1.3 × 1.3 × 5.0 mm^3).
B. DL image was obtained using BLADE (3; 55 seconds; 288 × 288; 7/8; 1.3 × 1.3 × 5.0 mm^3) with a research DL reconstruction. Both images display mild focal dilatation of B5 with improved bile duct sharpness, reduced image noise, and decreased image acquisition time dramatically using DL compared to those using conventional T2 BLADE without DL reconstruction (A).
DL = deep-learning, GRAPPA = generalized auto-calibrating partially parallel acquisition

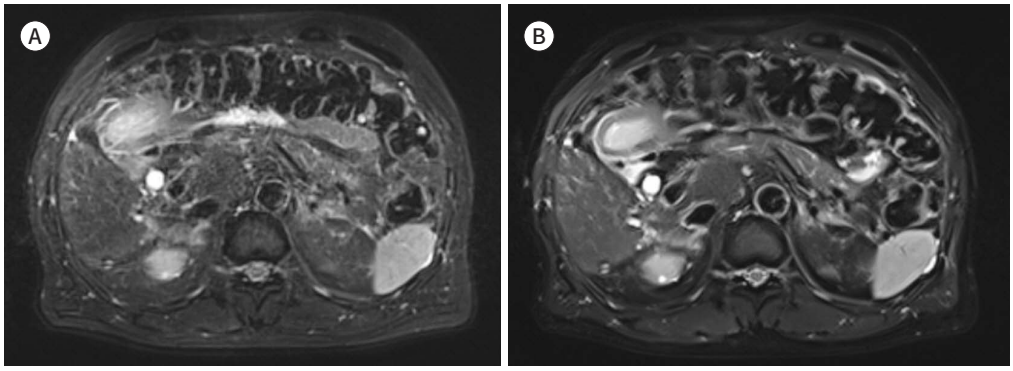

Boost; Siemens Healthineers, Erlangen, Germany). Additionally, DL techniques contribute to the improvement of image quality and reduce the scan time. AIR™ Recon DL (ARDL; GE Healthcare) is another DL-based reconstruction method designed to enhance image sharpness by eliminating truncation artifacts and simultaneously denoising an image to improve quality (25). DL-based reconstruction method applies a convolutional neural network (CNN) to an image reconstruction pipeline using raw k-space data to produce high-data-consistency images (25). The CNN is trained in a supervised manner to generate high-resolution data with minimal ringing artifacts and extremely low image noise levels. A few studies have successfully applied DL single-shot sequences, such as half-Fourier acquisition single-shot turbo spin-echo (HASTE) or T2-weighted sequences, to the upper abdomen (24, 27). DL-HASTE, SSFSE, and contrast-enhanced T1-weighted sequences provide a balanced combination of image quality and relatively short scan times (27-29). Another novel noise-reduction technique, utilizing the physical driven-DL (i.e., Adaptive-CS-Net) reconstruction method, artificial intelligence (Philips Healthcare), has been introduced to significantly improve image quality (30). This CNN is trained for all contrasts and a wide range of acceleration factors and outperforms conventional general sparsity representations, such as the wavelet transformation implemented in Compressed SENSE (SENSE + CS, Philips Healthcare).

When adopting DL reconstruction for diffusion-weighted imaging (DWI), the image displays better overall quality, sharpness of the organ margins, and fewer artifacts than conventional DWI (27, 31). In conventional DWI, the left lobe of the liver is vulnerable to cardiac motion artifacts, and the presence of bowel gas adjacent to the pancreas causes susceptibility artifacts that affect the pancreatic image quality. (Figs. 10, 11) (31).

MULTI-ARTERIAL PHASE IN A SINGLE BREATH-HOLD

Dynamic T1-weighted imaging (T1WI), which provides dynamic and hepatobiliary phases,

JOURNAL of THE KOREAN SOCIETY of RADIOLOGY

is the most important sequence in liver MRI for determining focal lesions. However, liver MRI using hepatocyte-specific contrast agents (e.g., gadoxetic acid) has some unpredictable challenges, including transient severe motion and a short arterial window compared to extracellular contrast media (2). Prolonged scanning times and gadoxetic acid-induced respiratory motion artifacts in the late arterial phase are problematic. For these reasons, several attempts, such as multiple arterial phase imaging with parallel imaging, CAIPIRINHA, CS, a hybrid of parallel imaging and CS, and DL, have been made to obtain an optimal arterial phase image without significant motion artifacts (Fig. 3) (10, 32-35). Multiple arterial phase acquisitions have displayed reduced transient severe motion artifacts in the arterial phase of liver MRI, providing a well-timed, late hepatic arterial phase image (10, 32, 34, 35). Moreover, using a hybrid of parallel imaging and CS, T1-weighted dynamic images that are sparse in the temporal domain can be obtained with a thin slice and acceptable image quality (Fig. 12). This enables acceleration factors greater than four and at the same time acquisition times less than 10 seconds while maintaining fair image quality (5).

Fig. 10. Dynamic phases in gadoxetic acid-enhanced liver MRI and diffusion-weighted imaging, apparent diffusion coefficient map using deep-learning in liver MRI in a 54-year-old male with liver cirrhosis.
Approximately 1 cm nodule in segment six radiologically probable hepatocellular carcinoma displays arterial phase hyperenhancement with washout on portal venous phase (not displayed).
A, B. DWI (b = 900 sec/mm^2) and ADC map were obtained using a research DL reconstruction (GRAPPA; acceleration factor 3; 119 s; matrix 140 × 140, reconstruction voxel size, 1.4 × 1.4 × 5.0 mm^3; k-space based DL reconstruction combined with image-based super-resolution).
C, D. DWI and ADC maps were obtained without DL reconstruction (GRAPPA; acceleration factor 3; 209 seconds; matrix 140 × 140, reconstructed voxel size, 2.7 × 2.7 × 5.0 mm^3). The DL DWI and ADC map demonstrates improved conspicuity of the focal lesion (arrow in A-D) and clearer edges, with reduced image noise, despite a dramatically decreased image acquisition time, compared to conventional DWI and ADC maps.
ADC = apparent diffusion coefficient, DL = deep-learning, DWI = diffusion-weighted imaging, GRAPPA = generalized auto-calibrating partially parallel acquisition

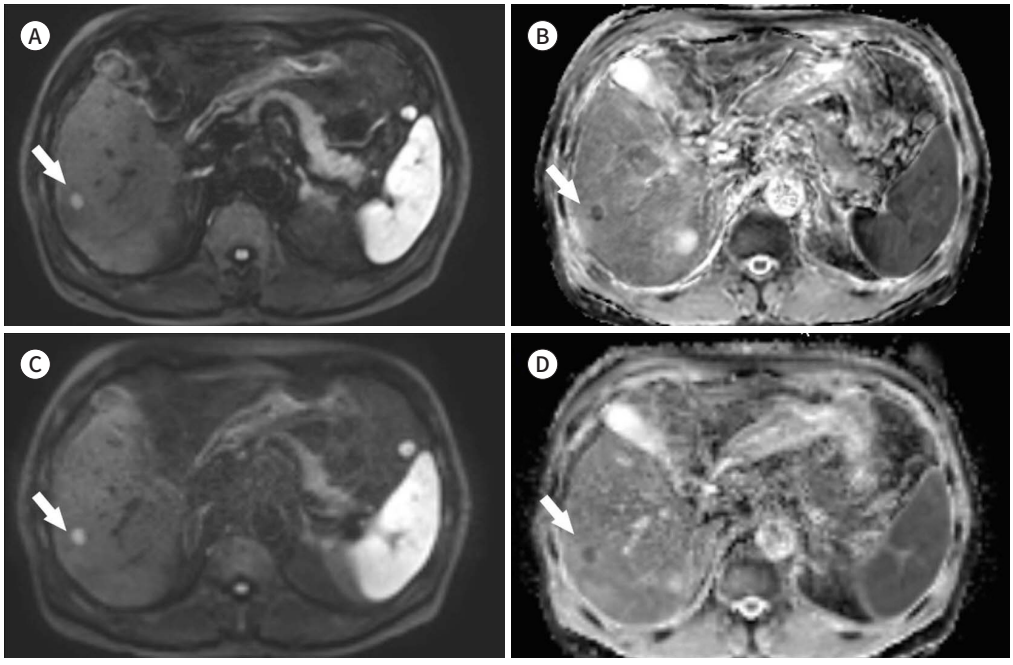

Fig. 11. Free-breathing diffusion-weighted imaging, apparent diffusion coefficient map using motion correction in liver MRI in a 48-year-old male with chronic hepatitis B.
A-D. Free-breathing DWI and ADC map were obtained with motion correction (A, B) DWI and ADC map were obtained without motion correction (C, D). Although both images display comparable overall image quality, (A) the image displays more distinct liver edge sharpness and clarity, even at the left lateral segment (arrows) as well as hepatic vessel clarity compared with a mild blur of liver edge and hepatic vessel on (C) image.
ADC = apparent diffusion coefficient, DWI = diffusion-weighted imaging

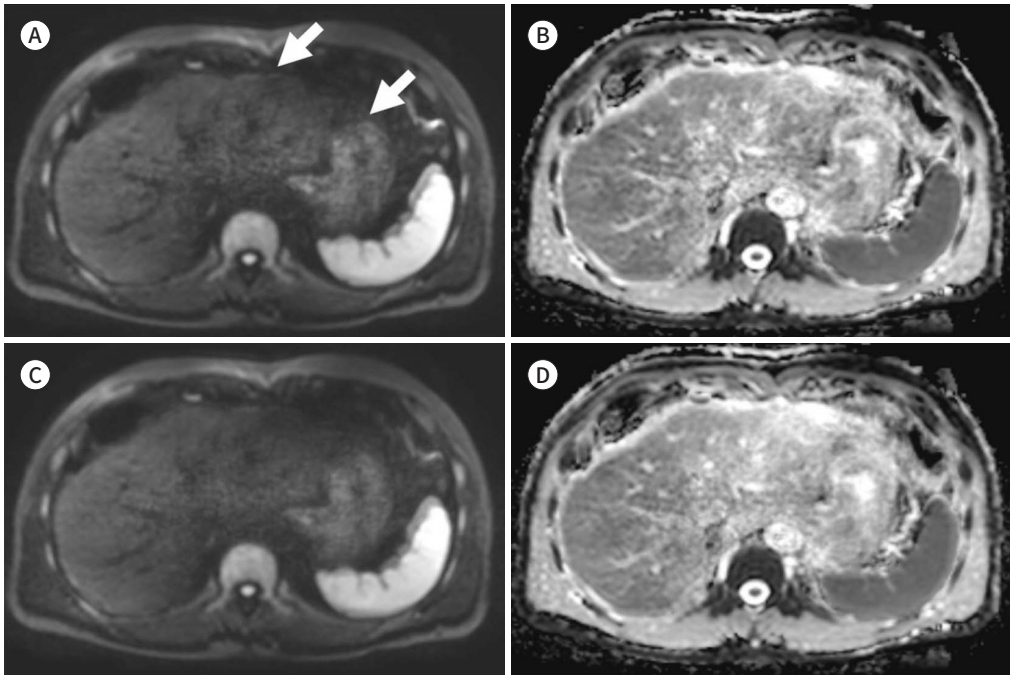

FREE-BREATHING T1-WEIGHTED IMAGE

As previously discussed, several techniques for reducing the scan time have been developed while preserving acceptable image quality. However, challenges related to motion, such as limited breath-holding capacity, may result in motion artifacts. Free-breathing techniques may provide a solution for patients who have difficulty holding their breath for prolonged periods or those who are under sedation, as well as for those who are at risk of motion artifacts in liver dynamic phase imaging. Free-breathing T1WI using either Cartesian (extra-dimensional-volumetric interpolated breath-hold examination; XD-VIBE) or radial acquisitions (golden-angle radial sparse parallel; GRASP, Siemens Healthineers, Erlangen, German); liver acceleration volume acquisition (LAVA) Star (GE Healthcare); differential sub-sampling with Cartesian ordering (DISCO) Star (GE Healthcare); 3D Vane XD (Philips Healthcare); 4D Free-Breathing (Philips Healthcare) has been introduced (36, 37). These techniques enable continuous acquisition of data and can be applied to retrospective motion correction. This motion-robust technique may assist patients with poor breath-holding capacity, reducing the chances of reexamination due to motion artifacts.

As Cartesian acquisition is more vulnerable to motion than radial acquisition, motion compensation using XD reconstruction is used in free-breathing Cartesian acquisition to maintain image quality (Figs. 13, 14) (38, 39). Radial acquisitions such as GRASP are inherently less susceptible to motion (Figs. 15, 16) (5). Given that the central region of the k-space is sampled

JOURNAL of THE KOREAN SOCIETY of RADIOLOGY

Fig. 12. Triple arterial phase images in a 45-year-old male with liver cirrhosis and chronic hepatitis C.
All images were from a research application that combines CAIPIRINHA and CS imaging with a total acceleration factor of 14 (CAIPIRINHA Acceleration factor 4; acceleration factor phase encoding 2, acceleration factor 3D 2, reordering shift 3D 1, CS acceleration factor 3.5).
A. The first image was obtained in the first arterial phase.
B. The next image was from the second arterial phase.
C. The third image was obtained in the third arterial phase. Image acquisition time is 19 seconds in total including a preparation scan of 1 second, and three arterial phases (each 6 seconds, respectively).
D-F. Subtraction arterial phase images were reconstructed using (A-C) images and pre-contrast images (not displayed) in each arterial phase. Images display excellent image quality and spatial resolution (reconstructed voxel size: 0.5 × 0.5 × 1.2 mm^3), without motion artifacts.
CAIPIRINHA = controlled aliasing in parallel imaging results in higher acceleration, CS = compressed sensing

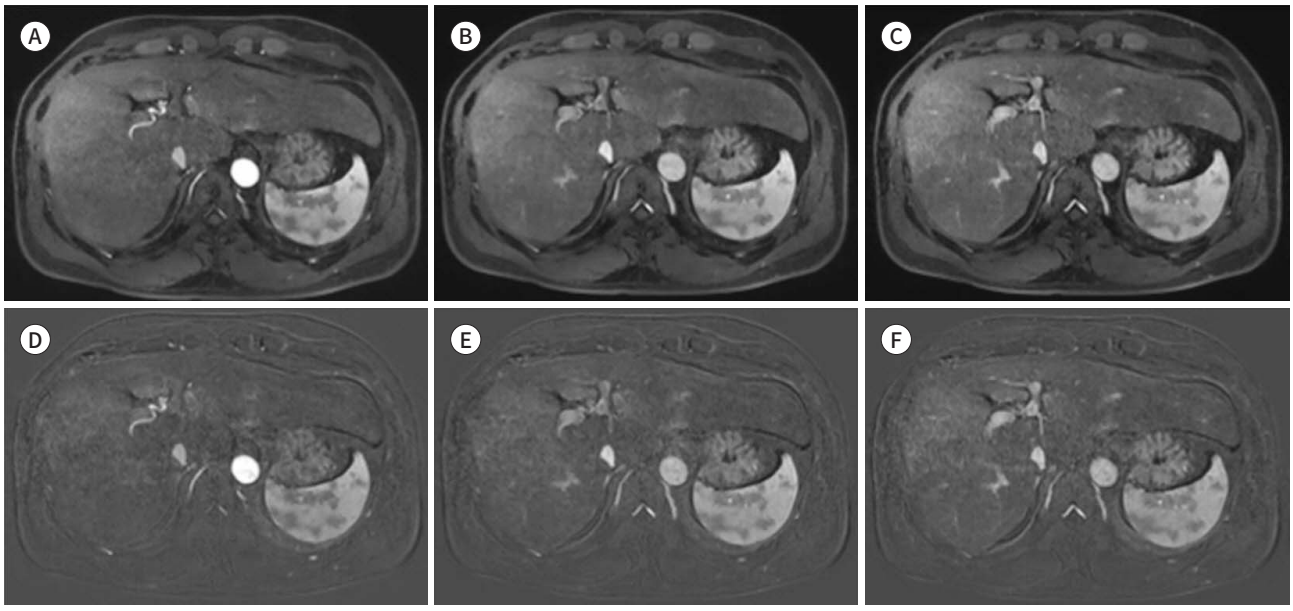

Fig. 13. Free-breathing dynamic phases in gadoxetic acid-enhanced liver MRI using XD-VIBE in a 74-year-old male.
Due to the non-cooperative state of the patient, images were obtained with the XD-VIBE research application (compressed sensing; acceleration factor, 5; temporal resolution, 12.5 seconds; the number of measurements, 18; total time, 225 seconds; matrix 352 × 224; reconstruction voxel size, 1.1 × 1.1 × 3.0 mm^3) and continuous dynamic MR images in the free-breathing state.
A-E. Pre (A), arterial (B), portal (C), and transitional phase (D) MR images display a mass of 4 cm approximately in segment four with gradual centripetal fill-in enhancement and (E) hepatobiliary phase hypointensity, which suggests a hemangioma.
XD-VIBE = extra-dimensional-volumetric interpolated breath-hold examination

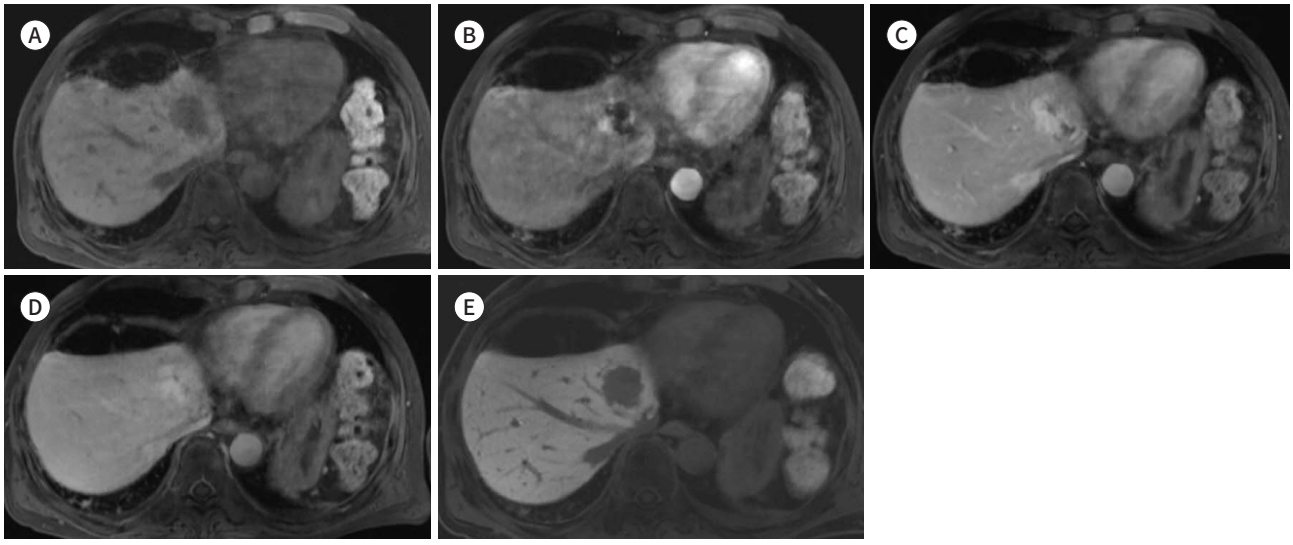

Fig. 14. Free-breathing dynamic phases in gadoxetic acid-enhanced liver MRI using XD-VIBE in 92-year-old female.
Images were obtained with the XD-VIBE research application (compressed sensing; acceleration factor 5; temporal resolution 12.5 seconds; total 225 seconds; matrix 352 × 224, reconstructed voxel size, 1.1 × 1.1 × 3.0 mm^3), a Cartesian acquisition which is relatively sensitive to motion compared with GRASP. Due to its drawback, continuously acquired dynamic MR images in the free-breathing state.
A-C. Pre (A), arterial (B), and portal phase (C) display moderate respiratory motion artifacts.
GRASP = golden-angle radial sparse paralle, XD-VIBE = extra-dimensional-volumetric interpolated breath-hold examination

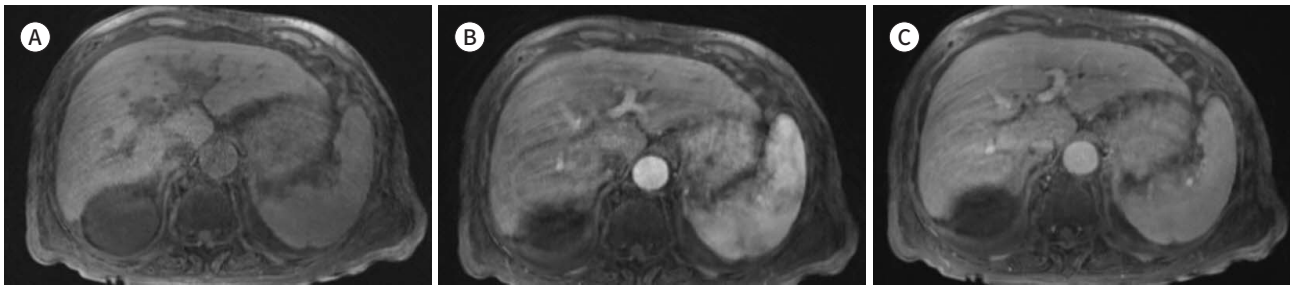

Fig. 15. Free-breathing dynamic phases in gadoxetic acid-enhanced liver MRI using SG-GRASP in an 84-year-old female with liver cirrhosis.
As the patient had a short breath-holding capability, the patient underwent continuous dynamic MR images in the free-breathing state during the injection of gadoxetic acid at a rate of 1.6 mL/s. Images were from SG-GRASP (50% of expiratory phase data based on SG motion state, radial spoke, 44; temporal resolution, 13 seconds; matrix 352 × 352).
A-C. Pre (A), arterial (B), and portal phase (C) MR images are acceptable without respiratory motion artifacts and display a 3 cm mass in segment seven with arterial phase hyperenhancement (B, arrow) and washout on portal venous phase (C, arrow), suggesting hepatocellular carcinoma.
SG-GRASP = self-gated golden-angle radial sparse parallel

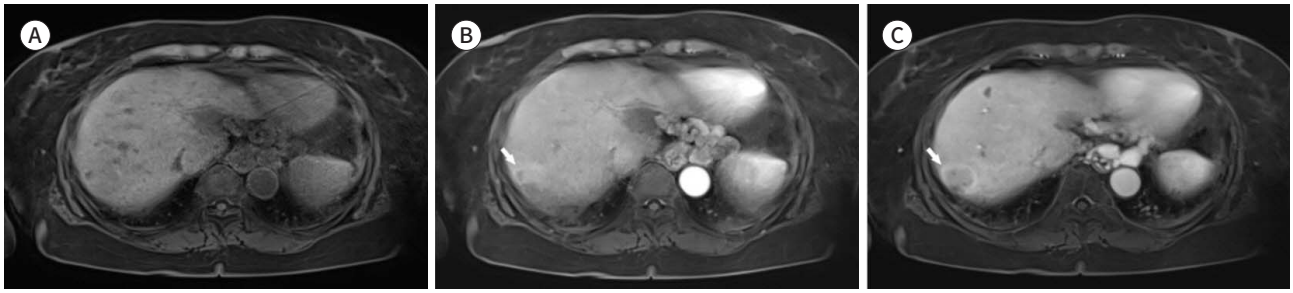

Fig. 16. Free-breathing dynamic phases in gadoxetic acid-enhanced liver MRI using SG-GRASP in an 80-year-old female with liver cirrhosis.
Images were obtained with SG-GRASP (50% of expiratory phase data based on SG motion state, radial spoke, 44; temporal resolution, 13 seconds; matrix 352 × 352) and continuous dynamic MR images in the free-breathing state during injection of gadoxetic acid at a rate of 1.6 mL/s.
A-C. Pre (A), arterial (B), and portal phase (C) MR images display a mass of approximately 1 cm in segment two with arterial phase hyperenhancement (B, arrow) and washout on portal venous phase (C, arrow) suggesting hepatocellular carcinoma. Images are acceptable without respiratory motion artifacts, but mild streak artifacts.
SG-GRASP = self-gated golden-angle radial sparse parallel

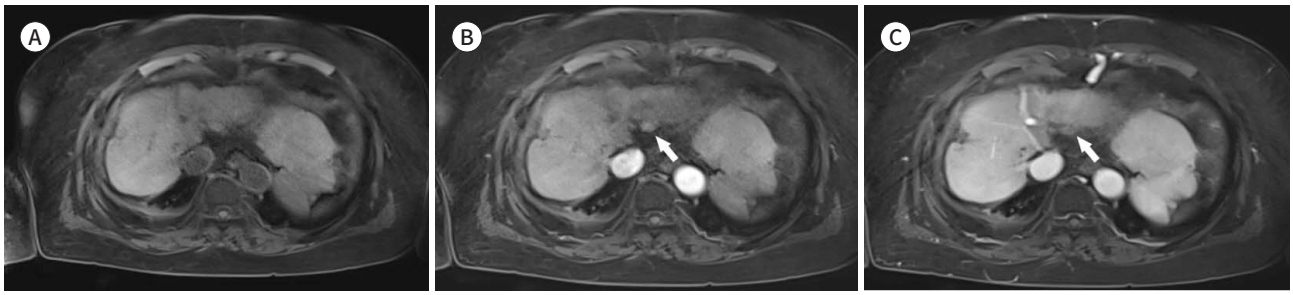

JOURNAL of THE KOREAN SOCIETY of RADIOLOGY

with every spoke in radial sampling, it allows for the possibility of retrospective respiratory self-gating. This enables the selection of the expiratory phase for image reconstruction, reducing motion artifacts. However, this method can potentially introduce streak artifacts and reduce margin sharpness. Radial k-space data sampling uses the golden-angle scheme along a time series by grouping a random number of consecutive spokes into temporal frames (40). The golden angle indicates that the radial line angles increase continuously by 111.25°, which causes the radial lines to be evenly spaced over time (41). Obtaining k-space coverage that is relatively uniform with high temporal inconsistency regardless of the number of spokes facilitates continuous data acquisition during dynamic imaging and the retrospective reconstruction of images with a certain temporal resolution by sorting selected numbers of spokes for time grouping (40).

LAVA, DISCO Star, 3D Vane XD, and 4D free breathing also use radial acquisition by stack-of-stars sampling (42). In addition, 3D Vane XD is a 3D gradient echo sequence with pseudo-golden-angle radial acquisition, which adds fine adjustments, resulting in every radial line being evenly spaced over time (43). The 4D free-breathing sequence is also motion-robust through respiratory soft gating and is compatible with high-precision external sensors. This sequence acquires images throughout all respiratory phases, not limited to the expiratory phase, and reconstructs the images using weighting factors based on motion levels. However, radial acquisition may generate different types of artifacts such as streaks, local blurring, heterogeneous

Fig. 17. Free-breathing dynamic phases in gadoxetic acid-enhanced liver MRI using SG-GRASP in an 88-year-old female with chronic hepatitis C. Images were obtained with SG-GRASP (50% of expiratory phase data-based on SG motion state, radial spoke, 44; temporal resolution, 13 seconds; matrix 352 × 352) and continuous dynamic MR images in the free-breathing state during injection of gadoxetic acid at a rate of 1.6 mL/s.
A-F. Superior segments of pre (A), arterial (B), portal phase (C) MR images and inferior segments of pre (D), arterial (E), and portal phase (F) MR images display good adequacy of arterial phase timing, (B) and (E) images display mild portal vein opacification with mild parenchymal enhancement, without hepatic venous enhancement, suggestive of good late arterial phase images.
SG-GRASP = self-gated golden-angle radial sparse parallel

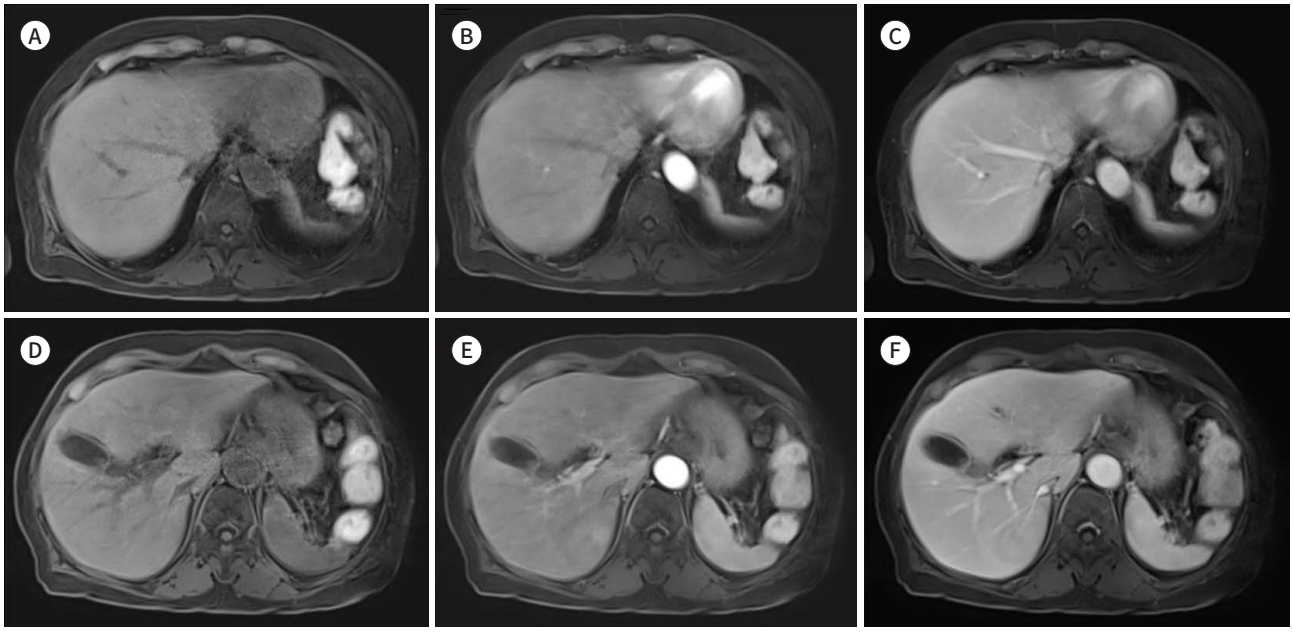

Fig. 18. Free-breathing dynamic phases in gadoxetic acid-enhanced liver MRI using SG-GRASP in a 91-year-old female.
Images were obtained with SG-GRASP (50% of expiratory phase data based on SG motion state, radial spoke, 44; temporal resolution, 13 seconds; matrix 352 × 352; time axis regularization factor 20) and continuous dynamic MR images in the free-breathing state during injection of gadoxetic acid at a rate of 1.6 mL/s.
A-C. Superior segments of pre (A), late arterial (B), and portal phase (C) MR images display too late arterial phase timing. (B) The image displays hepatic venous enhancement, suggestive of hepatic vein contamination in the late arterial phase due to k-space sharing.
SG-GRASP = self-gated golden-angle radial sparse parallel

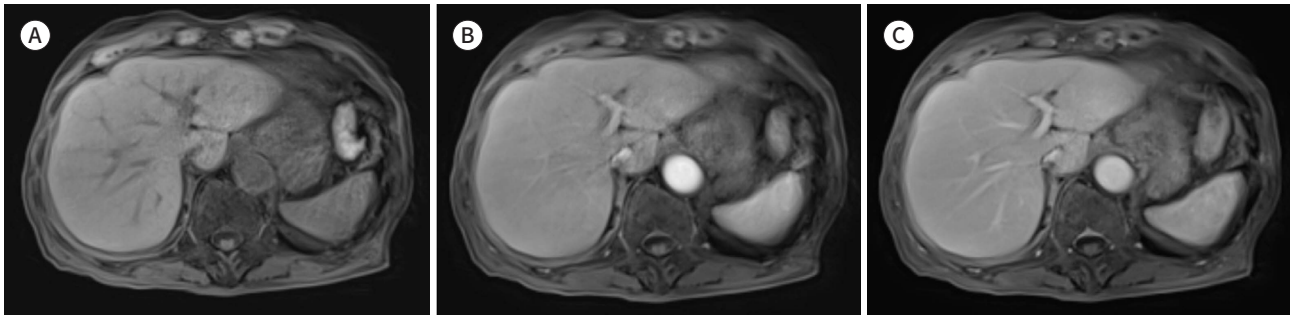

textures, or unusual imaging appearances (Fig. 16) (38).

Both free-breathing T1WI techniques can obtain late arterial phases and other dynamic images (Figs. 13, 17). However, a few images may demonstrate a suboptimal late arterial phase due to venous contamination, displaying hepatic venous enhancement and too weak or too strong parenchymal enhancement (Fig. 18) (44).

CONCLUSION

Currently, MRI plays a major role in the medical field because of the comprehensive and accurate diagnostic information. However, long scan times, non-cooperative patients, and hepatocyte-specific contrast agent-related problems are challenging factors. Numerous innovative techniques have been developed to accelerate MRI and overcome these limitations. In this study, we review several techniques for reducing scan time, including parallel imaging, CS, DL, and free-breathing techniques. In MRI, a trade-off always exists between the acquisition time, image resolution, and SNR. However, radiologists should be aware of a variety of techniques to provide the best MRI image quality for any patient as well as to interpret the sequences appropriately.

Author Contributions

Conceptualization, P.S.H.; formal analysis, L.Y.; software, N.M.D.; writing—original draft, L.Y.; and writing—review & editing, Y.S., P.S.H., N.M.D.

Conflicts of Interest

Nickel, Marcel Dominik is an employee of Siemens Healthcare GmbH. All remaining authors have declared no conflicts of interest.

ORCID iDs

Yoonhee Lee https://orcid.org/0000-0002-5266-4322
Sungjin Yoon https://orcid.org/0000-0002-7030-841X
So Hyun Park https://orcid.org/0000-0001-9935-2863
Marcel Dominik Nickel https://orcid.org/0000-0002-0360-7233

Funding

None

Acknowledgments

The authors would like to thank JaeKon Sung, MunYoung Paek, Dongyeob Han, Joonsung Lee, and Sang-Young Kim for their support throughout this project.

REFERENCES

1. Canellas R, Rosenkrantz AB, Taouli B, Sala E, Saini S, Pedrosa I, et al. Abbreviated MRI protocols for the abdomen. *Radiographics* 2019;39:744-758
2. Huh J, Kim SY, Yeh BM, Lee SS, Kim KW, Wu EH, et al. Troubleshooting arterial-phase MR images of gadoxetate disodium-enhanced liver. *Korean J Radiol* 2015;16:1207-1215
3. Ichikawa S, Motosugi U, Sato K, Shimizu T, Wakayama T, Onishi H. Transient respiratory-motion artifact and scan timing during the arterial phase of gadoxetate disodium-enhanced MR imaging: the benefit of shortened acquisition and multiple arterial phase acquisition. *Magn Reson Med Sci* 2021;20:280-289
4. Deshmane A, Gulani V, Griswold MA, Seiberlich N. Parallel MR imaging. *J Magn Reson Imaging* 2012;36:55-72
5. Yoon JH, Nickel MD, Peeters JM, Lee JM. Rapid imaging: recent advances in abdominal MRI for reducing acquisition time and its clinical applications. *Korean J Radiol* 2019;20:1597-1615
6. Yanasak NE, Kelly MJ. MR imaging artifacts and parallel imaging techniques with calibration scanning: a new twist on old problems. *Radiographics* 2014;34:532-548
7. Mukherjee P, Chung SW, Berman JI, Hess CP, Henry RG. Diffusion tensor MR imaging and fiber tractography: technical considerations. *AJNR Am J Neuroradiol* 2008;29:843-852
8. Hamilton J, Franson D, Seiberlich N. Recent advances in parallel imaging for MRI. *Prog Nucl Magn Reson Spectrosc* 2017;101:71-95
9. Nepal P, Bagga B, Feng L, Chandarana H. Respiratory motion management in abdominal MRI: radiology in training. *Radiology* 2023;306:47-53
10. Park YS, Lee CH, Kim IS, Kiefer B, Woo ST, Kim KA, et al. Usefulness of controlled aliasing in parallel imaging results in higher acceleration in gadoxetic acid-enhanced liver magnetic resonance imaging to clarify the hepatic arterial phase. *Invest Radiol* 2014;49:183-188
11. Breuer FA, Blaimer M, Mueller MF, Seiberlich N, Heidemann RM, Griswold MA, et al. Controlled aliasing in volumetric parallel imaging (2D CAIPIRINHA). *Magn Reson Med* 2006;55:549-556
12. Lustig M, Donoho D, Pauly JM. Sparse MRI: the application of compressed sensing for rapid MR imaging. *Magn Reson Med* 2007;58:1182-1195
13. Yoon S, Shim YS, Park SH, Sung J, Nickel MD, Kim YJ, et al. Hepatobiliary phase imaging in cirrhotic patients using compressed sensing and controlled aliasing in parallel imaging results in higher acceleration. *Eur Radiol* 2024;34:2233-2243
14. Feng L, Benkert T, Block KT, Sodickson DK, Otazo R, Chandarana H. Compressed sensing for body MRI. *J Magn Reson Imaging* 2017;45:966-987
15. Yoon S, Park SH, Han D. Uncover this tech term: compressed sensing magnetic resonance imaging. *Korean J Radiol* 2023;24:1293-1302
16. Sandino CM, Cheng JY, Chen F, Mardani M, Pauly JM, Vasanawala SS. Compressed sensing: from research to clinical practice with deep neural networks: shortening scan times for magnetic resonance imaging. *IEEE Signal Process Mag* 2020;37:111-127
17. Akasaka T, Fujimoto K, Yamamoto T, Okada T, Fushimi Y, Yamamoto A, et al. Optimization of regularization parameters in compressed sensing of magnetic resonance angiography: can statistical image metrics mimic radiologists' perception? *PLoS One* 2016;11:e0146548
18. Jaspan ON, Fleysher R, Lipton ML. Compressed sensing MRI: a review of the clinical literature. *Br J Radiol* 2015;88:20150487
19. Song JS, Kim SH, Kuehn B, Paek MY. Optimized breath-hold compressed-sensing 3D MR cholangiopancreatography at 3T: image quality analysis and clinical feasibility assessment. *Diagnostics (Basel)* 2020;10:376
20. Zhu L, Xue H, Sun Z, Qian T, Weiland E, Kuehn B, et al. Modified breath-hold compressed-sensing 3D MR cholangiopancreatography with a small field-of-view and high resolution acquisition: clinical feasibility in

biliary and pancreatic disorders. *J Magn Reson Imaging* 2018;48:1389-1399
21. Yoon JH, Lee SM, Kang HJ, Weiland E, Raithel E, Son Y, et al. Clinical feasibility of 3-dimensional magnetic resonance cholangiopancreatography using compressed sensing: comparison of image quality and diagnostic performance. *Invest Radiol* 2017;52:612-619
22. Recht MP, Zbontar J, Sodickson DK, Knoll F, Yakubova N, Sriram A, et al. Using deep learning to accelerate knee MRI at 3 T: results of an interchangeability study. *AJR Am J Roentgenol* 2020;215:1421-1429
23. Wessling D, Herrmann J, Afat S, Nickel D, Almansour H, Keller G, et al. Application of a deep learning algorithm for combined super-resolution and partial fourier reconstruction including time reduction in T1-weighted precontrast and postcontrast gradient echo imaging of abdominopelvic MR imaging. *Diagnostics (Basel)* 2022;12:2370
24. Gassenmaier S, Küstner T, Nickel D, Herrmann J, Hoffmann R, Almansour H, et al. Deep learning applications in magnetic resonance imaging: has the future become present? *Diagnostics (Basel)* 2021;11:2181
25. Lebel RM. Performance characterization of a novel deep learning-based MR image reconstruction pipeline. arXiv [Preprint]. 2020 [cited 2023 August 1]. Available at. https://doi.org/10.48550/arXiv.2008.06559
26. Kaji S, Kida S. Overview of image-to-image translation by use of deep neural networks: denoising, super-resolution, modality conversion, and reconstruction in medical imaging. *Radiol Phys Technol* 2019;12:235-248
27. Zerunian M, Pucciarelli F, Caruso D, Polici M, Masci B, Guido G, et al. Artificial intelligence based image quality enhancement in liver MRI: a quantitative and qualitative evaluation. *Radiol Med* 2022;127:1098-1105
28. Herrmann J, Gassenmaier S, Nickel D, Arberet S, Afat S, Lingg A, et al. Diagnostic confidence and feasibility of a deep learning accelerated HASTE sequence of the abdomen in a single breath-hold. *Invest Radiol* 2021;56:313-319
29. Son JH, Lee Y, Lee HJ, Lee J, Kim H, Lebel MR. LAVA HyperSense and deep-learning reconstruction for near-isotropic (3D) enhanced magnetic resonance enterography in patients with Crohn's disease: utility in noise reduction and image quality improvement. *Diagn Interv Radiol* 2023;29:437-449
30. Pezzotti N, Yousefi S, Elmahdy MS, Van Gemert JHF, Schuelke C, Doneva M, et al. An adaptive intelligence algorithm for undersampled knee MRI reconstruction. *IEEE Access* 2020;8:204825-204838
31. Bae SH, Hwang J, Hong SS, Lee EJ, Jeong J, Benkert T, et al. Clinical feasibility of accelerated diffusion weighted imaging of the abdomen with deep learning reconstruction: comparison with conventional diffusion weighted imaging. *Eur J Radiol* 2022;154:110428
32. Pietryga JA, Burke LM, Marin D, Jaffe TA, Bashir MR. Respiratory motion artifact affecting hepatic arterial phase imaging with gadoxetate disodium: examination recovery with a multiple arterial phase acquisition. *Radiology* 2014;271:426-434
33. Kim DW, Choi SH, Park T, Kim SY, Lee SS, Byun JH. Transient severe motion artifact on arterial phase in gadoxetic acid-enhanced liver magnetic resonance imaging: a systematic review and meta-analysis. *Invest Radiol* 2022;57:62-70
34. Yoon JK, Kim MJ, Lee S. Compressed sensing and parallel imaging for double hepatic arterial phase acquisition in gadoxetate-enhanced dynamic liver magnetic resonance imaging. *Invest Radiol* 2019;54:374-382
35. Kim JH, Yoon JH, Bae JS, Park S, Han S, Lee JM. Multiarterial phase acquisition in gadoxetic acid–enhanced liver MRI for the detection of hypervascular hepatocellular carcinoma in high-risk patients: comparison of compressed sensing versus view sharing techniques. *Invest Radiol* 2023;58:139-147
36. Park SH, Yoon JH, Park JY, Shim YS, Lee SM, Choi SJ, et al. Performance of free-breathing dynamic T1-weighted sequences in patients at risk of developing motion artifacts undergoing gadoxetic acid-enhanced liver MRI. *Eur Radiol* 2023;33:4378-4388
37. Allen BC, Ehieli WL, Wildman-Tobriner B, Chaudhry M, Bozdogan E, Janas G, et al. DIfferential subsampling with cartesian ordering with respiratory triggering versus conventional liver acquisition with volume acquisition: a multiple reader preference study. *J Comput Assist Tomogr* 2019;43:623-627
38. Yoon JH, Yu MH, Chang W, Park JY, Nickel MD, Son Y, et al. Clinical feasibility of free-breathing dynamic T1-weighted imaging with gadoxetic acid–enhanced liver magnetic resonance imaging using a combination of variable density sampling and compressed sensing. *Invest Radiol* 2017;52:596-604
39. Kaltenbach B, Bucher AM, Wichmann JL, Nickel D, Polkowski C, Hammerstingl R, et al. Dynamic liver magnetic resonance imaging in free-breathing: feasibility of a Cartesian T1-weighted acquisition technique with compressed sensing and additional self-navigation signal for hard-gated and motion-resolved reconstruction. *Invest Radiol* 2017;52:708-714

JOURNAL of THE KOREAN SOCIETY of RADIOLOGY

40. Feng L, Grimm R, Block KT, Chandarana H, Kim S, Xu J, et al. Golden-angle radial sparse parallel MRI: combination of compressed sensing, parallel imaging, and golden-angle radial sampling for fast and flexible dynamic volumetric MRI. *Magn Reson Med* 2014;72:707-717
41. Winkelmann S, Schaeffter T, Koehler T, Eggers H, Doessel O. An optimal radial profile order based on the Golden Ratio for time-resolved MRI. *IEEE Trans Med Imaging* 2007;26:68-76
42. Ichikawa S, Motosugi U, Wakayama T, Morisaka H, Funayama S, Tamada D, et al. An intra-individual comparison between free-breathing dynamic MR imaging of the liver using stack-of-stars acquisition and the breath-holding method using cartesian sampling or view-sharing. *Magn Reson Med Sci* 2023;22:221-231
43. Kajita K, Goshima S, Noda Y, Kawada H, Kawai N, Okuaki T, et al. Thin-slice free-breathing pseudo-golden-angle radial stack-of-stars with gating and tracking T1-weighted acquisition: an efficient gadoxetic acid-enhanced hepatobiliary-phase imaging alternative for patients with unstable breath holding. *Magn Reson Med Sci* 2019;18:4-11
44. Yoon JH, Lee JM, Yu MH, Hur BY, Grimm R, Block KT, et al. Evaluation of transient motion during gadoxetic acid–enhanced multiphasic liver magnetic resonance imaging using free-breathing golden-angle radial sparse parallel magnetic resonance imaging. *Invest Radiol* 2018;53:52-61

복부 자기공명영상 고급 기법과 문제 해결 전략

이윤희[1] · 윤성진[1] · 박소현[1*] · Marcel Dominik Nickel[2]

자기공명영상(이하 MRI)은 복부 영상에서 국소 병변의 감지와 특성을 찾을 수 있는 것 때문에 중요한 역할을 한다. 그러나 MRI 검사에 상대적으로 긴 검사 시간과 호흡 유지 기법에서 움직임 관리와 같은 몇 가지 힘든 요인이 있다. 최근에는 검사 시간을 줄이면서 적절한 이미지 품질을 유지하는 기법인 평행 이미징, 압축 감지(compressed sensing) 및 최첨단 딥 러닝(deep learning) 기술이 등장하여 문제 해결 전략을 가능하게 하고 있다. 또한, 역동적 조영증강 영상에서 자유 호흡 기법은, 추가 차원(extra-dimensional)-부피 보간 호흡 유지 검사(volumetric interpolated breath-hold examination) 및 황금 각도 방사형 희소 병렬(golden-angle radial sparse parallel), 간 가속 볼륨 획득(liver acceleration volume acquisition) 스타와 같은, 심한 호흡곤란이나 마취 중인 환자에게서 복부 MRI를 시행하는 것을 돕는다. 이 임상화보에서는 시간을 줄이면서도 이미지 품질을 유지하기 위한 다양한 고급 복부 MRI 기술과 역동적 영상을 위한 자유 호흡 기술을 제시하고 또한 이를 통한 예시들을 보여주고자 한다. 이러한 첨단 기법들의 고찰은 적용된 시퀀스의 적절한 해석에 도움을 줄 것이다.

[1]가천대학교 의과대학 길병원 영상의학과,
[2]Siemens Healthineers